4.2

ON THE PREDICTABILITY OF SUMMER MONSOON DEPRESSIONS OVER SOUTH ASIA: The Impact of Cloud-System-Resolving Modeling

Yi-Chi Wang* and Wen-wen Tung

Department of Earth and Atmospheric Sciences, Purdue University,

West Lafayette, Indiana

1. INTRODUCTION

Monsoon depressions (MDs), which are among the major rainfall-producing systems during the Indian summer monsoon, have drawn a lot of attention because of their societal and economic impacts. Understanding of the excitation and maintaining mechanisms of the MDs is indispensible to the improvement of their dynamical predictability. In early studies such as Krishnamurti et al. (1975, 1976, and 1977) and Sikka (1977), characteristics of MDs such as the frequency of occurrence, structures, and propagation had been documented. However, it was not until the summer Monsoon Experiment (MONEX, 1979) that more detailed studies on the structure and dynamics of the MDs were accomplished (e.g., Nitta and Masuda, 1981; Warner, 1984; Douglas et al., 1992). Still, controversies arose in these studies, especially in terms of thermodynamic and dynamic features around the core of the MDs and, hence, the mechanisms sustaining them.

Moreover, the Asian monsoon is well known to be multiscale in space and time. A typical MD embedded in the monsoon mean flow has a horizontal spatial scale of several thousand kilometers, while about a quarter of it is vigorously convective. Previous theoretical and modeling studies had suggested that cumulus heating along with baroclinic and/or barotropic instability may be responsible for the growth and propagation of MDs (e.g., Krishnamurti et al., 1976; Shukla, 1978; Moorthi and Arakawa, 1985; Aravequia et al. 1995). Therefore, one question to ask is how the moist processes, in particular the moist convection, affects the predictive utility of a model in the case of the MD.

To address the above issues, high-resolution regional hindcasts focused on an intense MD in August 2006 were performed, using the Advanced Weather Research and Forecast (ARW) model. In this preliminary report we present 1) the improvement of the model's predictive utility resulted from resolving the cloud systems, and 2) the MD's core structure and possible reasons for the previous controversies

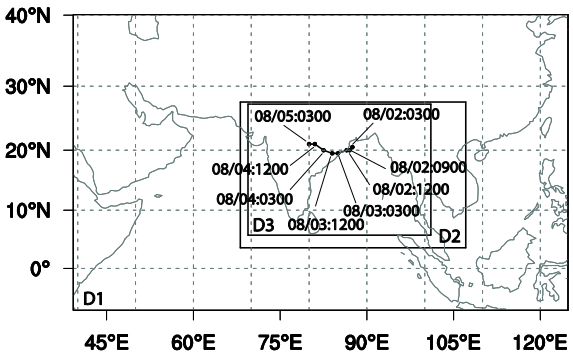

Figure 1 : The track of the monsoon depression with the observed time in IMD report (in Mausam, 2007) and the three-domain setup in WRF. The two-domain setup only includes D1 and D2.

2. OVERVIEW OF THE MONSOON DEPRESSION EVENT IN AUGUST 2006

Figure 1 shows the track of the MD investigated in this study. The track is determined according to the approximate center locations of the MD reported by the Indian Meteorological Department (IMD, in Mausam, 2007). The MD was first sighted as a low pressure system on August 1 over the northern tip of the Bay of Bengal (BoB). While deepening to a deep Depression on August 2, it propagated southwestward along the western coast of the BoB. This southward bend was considered as an unusual movement by the IMD. After that, it moved westward and made landfall at the coast of Orissa in the early morning of August 3. During August 4 to 5, the MD kept going westward over the central India. It weakened after turning northwestward on August 7 and eventually merged with the seasonal Low in Pakistan.

Figure 2a shows the 7-day averaged rain rate during August 1--7 calculated from the Tropical

Rainfall Measurement Mission (TRMM) 3B42 data (see Sec. 3). It is seen that the rainfall associated with the MD extends from the western BoB to Rajasthan. During the same period, a significant amount of rain is also observed over the mountainous range in the Western Ghats and off the coast of Burma. The rainfall maximum in an MD tends to concentrate in its southwest quadrant as it traverses the Indian subcontinent. Such asymmetry in the rainfall distribution is one of the major features of the MD as well as an important clue about its dynamics.

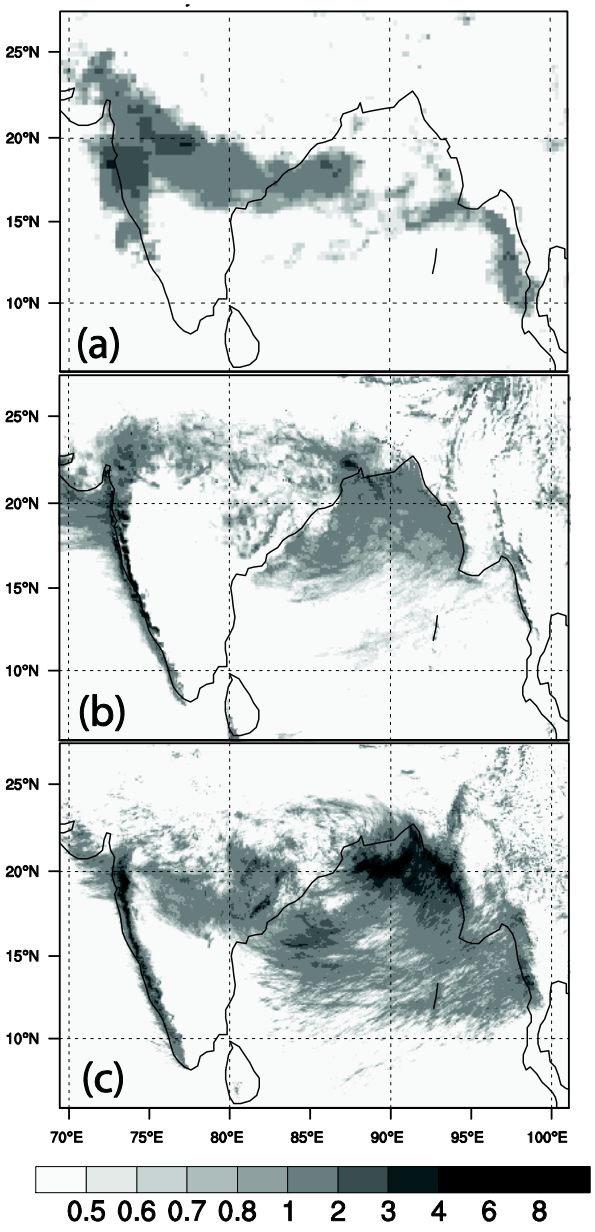

Figure 2 : Average rain rate (mm/hr) from a) TRMM 3B42, b) two-domain simulation, and c) three-domain simulation during Aug 1 to Aug 7, 2006.

3. METHODS AND DATA

3.1 The ARW Hindcast Experiments

The domain setups for both the ARW two-way two- and three-nested domains are shown in Figure 1. The outermost domain (D1) covered an area from 7° S to 40° N and from 40° E to 125° E, with 30-km horizontal resolution. The first inner domain (D2) was set up with 10-km resolution to better resolve the details of the MD. In addition to these two domains, a third domain (D3) with 3.33-km resolution was added for the three-domain experiment. In relation to the inner domains, the generous size of D1 was chosen so to ensure a most realistic simulation of the large-scale south Asian monsoon circulation and to keep the inner domains as far away from the model's lateral boundaries as possible.

The hindcast experiments utilized the WRF single-moment six-class microphysics scheme (Hong et al., 2004; Lin et al.,1983), the Noah land surface scheme (Chen and Dudhia, 2001), and the Yonsei University boundary layer scheme (Hong and Pan, 1996; Skamarock et al., 2005). The Rapid Radiative Transfer Model scheme (Mlawer et al, 1997) was used for the long-wave radiation while the MM5 Dudhia Shortwave scheme (Dudhia, 1989) was used for the short-wave radiations. The cumulus parameterization adopted for D1 and D2 was the Grell-Devenyi ensemble scheme (Grell and Devenyi, 2002), which performed superior to the Kain-Fristch (Kain and Fritsch, 1993) and Betts-Miller-Janjic (Janjic, 1994, 2000) schemes in a series of sensitivity runs. Cumulus parameterization was turned off in D3.

The integration of D1 was initialized from July 25 and ended at August 7, allowing sufficient time for the large-scale circulations to establish before the inner domains were activated. D2, as well as D3 in the three-domain experiment, was initialized on July 31. Analyses presented in the rest of the abstract are based on results between August 1 and August 7 in the hindcast experiments.

3.2 *Data*

Various operational analyses and reanalysis were tested as the initial and lateral boundary conditions for the 30-km D1 for the duration of 1 week. Results of these test runs showed that the combination of the six-hourly, 1.0° x 1.0°, NCEP Final (FNL) global analysis and the daily, 0.5° x 0.5°, NCEP Real-Time Global Sea Surface Temperature (RTG SST, Gemmill et al., 2007)

outperformed especially for hindcasting the track and precipitation of the MD.

Several observational datasets were used to validate the hindcasts. The six-hourly 2.5° x 2.5° NCEP/NCAR Reanalysis (Kalnay et al., 1996) provided the gross features of the monsoon circulations. The TRMM 3B42 was the major source of rain-rate validation. The 3B42 is a three-hourly, 0.25° x 0.25°, multi-satellite dataset produced by merging calibrated microwave and infrared precipitation estimates (Huffman et al., 1995, 1997; Huffman, 1997). The track of the observed MD was determined according to the IMD report (IMD, in Mausam, 2007) with the confirmation of the TRMM rain-rate and the NCEP/NCAR reanalysis. On the other hand, that of the hindcasted MD was determined with an automated algorithm which tracked the minima of the mean sea level pressure within the depression system.

4. RESULTS AND DISCUSSIONS

4.1 *The Predictability of Genesis and Track*

In both the two-domain and the three-domain (cloud-system resolving) experiments, the ARW captures the MD genesis in the BoB. This suggests high potential predictability for the MD genesis without the need to resolve the cloud systems. Therefore, the genesis of MD might be resulted from the hydrodynamic instability within the large-scale monsoon circulation.

Both ARW hindcasts reproduced the essential westward movement of the MD, however with faster propagation speeds than the IMD report. Within the 48 hours from 0300UTC on August 2, the MD propagated with a speed of ~3 m/s in the IMD report, while the propagation speeds are ~4—5 m/s in the two-domain experiment and ~4 m/s in the three-domain experiment. The discrepancy is mostly due to the accelerated propagation after the MD makes landfall in the hindcasts. The hindcasted systems appear to spend less than 2 days to cross the central India while in the observation it took 3 days (August 3—5) before it merged with the Pakistani low. As suggested in Fig. 2b, in the two-domain simulation the track deviates to the north so that the precipitating area is brought toward the foothills of the Himalayas. Such northward bias in the MD tracks has been reported in coarser-scale GCM studies (e.g., Sabre et al., 2000). On the other hand, the cloud-system-resolving simulation appears to place the MD track to locations conducive to precise forecast of precipitation (Fig. 2c).

4.2 *Precipitation Intensity and Distribution*

The precipitation hindcast can be addressed in terms of its intensity and spatial distribution. It is found that three-domain run better captures the overall intensity and the asymmetric distribution of precipitation, with rain rate maximum located over the southwest section and a relatively dry area over the northeast section (Fig. 2c). This is consistent with the TRMM observation (Fig. 2a) and previous observational studies. This wet/dry contrast is a significant feature of MD because the diabatic heating due to deep convection and downdraft cooling may influence the track of the depression. Although the wet/dry contrast is also shown in the two-domain simulation, the precipitating area is only loosely organized and far less concentrated than that in the observations. Even more, the rain rate maximum is wrongly placed to the north of the MD center after August 3.

It is noted that, as shown in Fig.2, both hindcasts appear to produce excessive precipitation over the Western Ghats and the BoB when compared with the TRMM observation. These are in fact stationary signals during the hindcast period. Although it has been found that the TRMM 3B42 tends to underestimate the rainfall over the Western Ghats (Nesbitt, personal communication), this may also imply the ARW's deficiency in simulating topographic rainfall. However, further studies are required to investigate this problem.

The better-simulated intensity and spatial distribution of the precipitation in the three-domain experiment is likely tied to its better hindcast of the MD track. Even though the coupling between organized deep convection and the larger-scale monsoon circulation may not be crucial for the genesis of the MD, the propagation of the MD and the downstream initiation of deep convection associated with it may be dictated by the multiscale interactions within the entire system including the monsoon mean flow, the synoptic MD circulation, and the organized deep convection. Krishnamurti et al. (1976) analyzed the energetics of a monsoon depression in a primitive equation model and suggested that cumulus convection was the primary driver of the disturbance. As our model resolution is increased from 10 km to the 3.33-km cloud-system-resolving scale, the energetics within the entire multiscale system may be better simulated; therefore, improved hindcast is obtained.

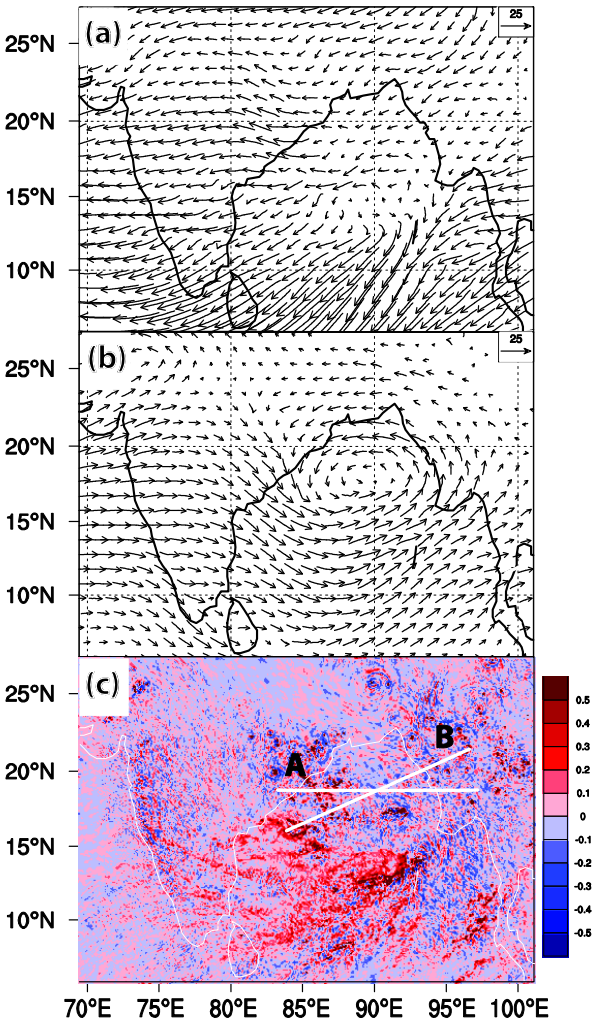

Figure 3 : Horizontal maps of wind fields within the 3-domain simulation at 0900UTC August 1st . (a) horizontal wind (m/s) fields at 200hPa level (b) horizontal wind (m/s) fields at 850hPa level (c) vertical velocity (m/s) at 300hPa level with black contours showing the precipitations.

4.3 *Core Structure*

In order to gain more understanding of the dynamics of the MD, the core structure of the simulated depression in the three-domain experiment is also examined. Here, the snapshot of the MD at 0900UTC on August 1 is shown as an example. At this time, the depression was over the BoB and in a similar stage of development with the depression investigated in summer MONEX (Krishnamurti et al., 1980). Figures 3a-c show the horizontal wind fields, vertical velocity, and precipitation associated with the MD. The 200-hPa wind field (Fig. 3a) shows that the strongest outflow of the MD is located on the southwest side of the low-level center of depression (Fig. 3b). The vertical velocity at 300 hPa (Fig. 3c) shows maximum convective ascends collocating with the maximum outflow at 200 hPa as well as maximum rainfall at the surface.

Figure 4a shows the thermal structure of the core of the MD with a longitudinal cross section (line A in Fig. 3c) of anomalous temperature and circulations. The anomalies are defined as the remains of a field after its time mean (August 1—7 in this case) and zonal mean (the longitudinal range of D3) are removed. Figure 4b shows the same fields except that the cross section is taken across the center of the MD and the nearest rain rate maximum (line B in Fig. 3c). In both Figs. 4a and b, the span of each cross section is approximately 1500 km with the depression center in the middle. This span is close to the horizontal scale of the very core of MD suggested in former studies (e.g., Krishnamurti et al., 1975). To produce these cross sections, ensemble averages have been performed over a range of approximately 200 km in the direction normal to the cross sections.

Figures 4a and 4b clearly show a strong horizontal gradient in the anomalous temperature over the lower levels from ~900 to 400 hPa as cold anomalies occupying to the southwest of the depression and warm anomalies to the northeast area. A vertical gradient of anomalous temperature is also most pronounced over the southwest area as the anomalously warm air extending to the southwest with increasing height (not shown). This extension is shown as a southwestward tilt of warm anomalies with height.

The circulation pattern in Figs. 4a and b show that the maximum ascending motion is about 100 km away from the center of the MD and is on its west (southwest) side. In Fig. 4a, the upward motion is concentrated above 350 hPa in the troposphere. The strong ascending motions from the surface to around 150 hPa are collocated with the rain rate maxima in Fig. 4b. In both Figs. 4a and b, over the east (northeast) part of the MD, relatively weak subsiding flows and intermittent weak upward motions are consistent with the relatively dry area of the depression as indicated by the low rain rate. At upper levels, both circulations and thermal structures indicate that the top of the MD is around 200 to 150 hPa as the easterly outflows become dominant on the west side and warm air anomalies recede.

Even though the cold anomalies in the thermal structure is collocated with the maximum ascending motion and rainfall in Fig. 4b, it is equally significant in 4a in which the ascending motion is only obvious in the upper troposphere and the rainfall is moderate.

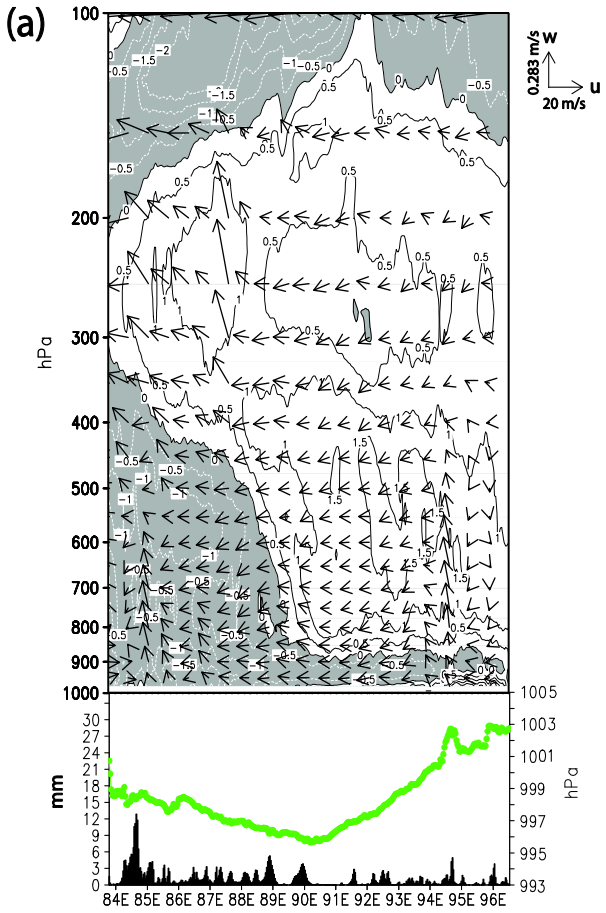

Figure 4: Cross sections of circulations (u,w : vectors) and temperature transient eddies (contours) through the depression core within the three-domain simulation at 0900UTC August 1st. Areas of negative temperature transient eddies are shaded. Units are m/s for wind fields and °C for temperature eddies. Precipitation (bins) and sea level pressure (dotted line) along cross sections are shown below with index indicating distance (in number of grid points) from the depression center. (a) Longitude-height section through the depression center (line A in fig3)

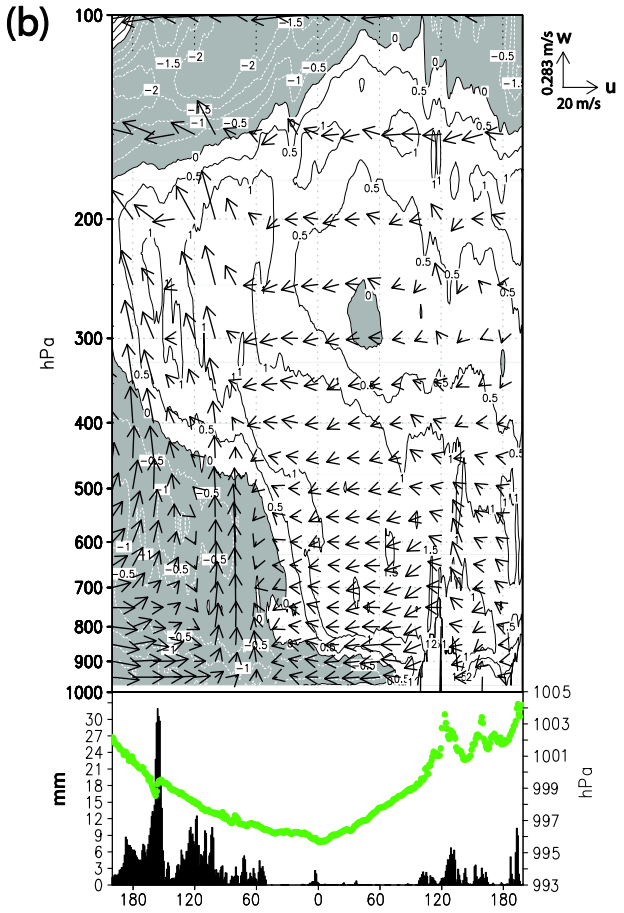

Figure 4(b): same as 4(a), except shows the cross section through the depression center and precipitating area (line B in fig3)

Therefore, the evaporative cooling in the precipitating downdraft may not be the only mechanism causing this vertical tilt. One conjecture is that the tilted structure observed here is associated with convection-coupled waves.

5. CONCLUDING REMARK

The monsoon depression event in August 2006 is simulated with the ARW model with two-way domain setup. With various observations including satellite imagery, radiosonde observations, and global reanalyses, it is found that its genesis and the subsequent westward propagation are captured in the hindcast of the two-domain setup. However, rainfall distribution and tracks of the monsoon depression still deviated from the observations from 24 hours after the MD had major rainfall over the BoB.

Intrigued by the sensitivity of simulation to the cumulus parameterizations, a 3.33-km domain is added to two-domain setup to resolve convection organizations. Impressive improvements are shown in terms of reproducing the precipitation asymmetry and south bend of the track before landfall in observations. Large deviation doesn't show up until 48 hours after the major rainfall starts. This improvement may be due to better simulated energetics with better resolved convection systems. The result further suggests the significance of the coupling between organized cloud systems and large-scale monsoon circulations for monsoon depression systems.

The core structure in the three-domain run is further examined and compared with findings in earlier studies. In terms of the controversy over the observed thermal structure, a southwestward tilt of warm core is found in the three-domain hindcast. This result shows better agreements with Douglas' study (1992) with the

analysis of summer MONEX, while opposing to the eastward tilt suggested by Krishnamurti et al. (1976) and Saha and Chang (1983). Detailed depicted circulations and thermal structure of the MD in the hindcast may further shed lights in issues such as the formation and propagation mechanisms of MDs.

With better agreements on rainfall distribution and the track of the simulated depression, the cloud-system-resolving hindcast in this study not only demonstrates improvements on predictability, but also shows a physically reasonable picture of core structure for the monsoon depression. Although better observations and studies are still needed for validations, it seems that cloud-system-resolving resolutions is worthy pursuing for better forecasts of the monsoon depression systems.

Acknowledgements. The authors would like to pay great gratitude to Dr. Dev Niyogi and Ms. H.-I. Chang for generously sharing their experiences in hindcasting monsoon depressions, and also to Drs. J. B. Gao, H.R. Hatwar, and Jui-Lin Li for their invaluable feedbacks. The computations are performed at the Purdue Rosen Center for Advanced Computing. This work is supported by NSF CMMI-0826119.

6. REFERENCES

Aravequia, J., V. Brahmananda Rao, and J. Bonatti, 1995: The Role of Moist Baroclinic Instability in the Growth and Structure of Monsoon Depressions. *J. Atmos. Sci.*, **52**, 4393–4409.

Chen, F., and J. Dudhia, 2001: Coupling an advanced land-surface/ hydrology model with the Penn State/ NCAR MM5 modeling system. Part I: Model description and implementation. *Mon. Wea. Rev*., **129**, 569–585.

Douglas, M.W., 1992: Structure and Dynamics of Two Monsoon Depressions. Part I: Observed Structure. *Mon. Wea. Rev.*, **120**, 1524–1547.

Dudhia, 1989: Numerical study of convection observed during the winter monsoon experiment using a mesoscale two-dimensional model, *J. Atmos. Sci.*, **46,** 3077-3107.

Gemmill, William, Bert Katz and Xu Li, 2007: Daily Real-Time Global Sea Surface Temperature - High Resolution Analysis at NOAA/NCEP. *NOAA / NWS / NCEP / MMAB Office Note* Nr. 260

Grell, G. A., and D. Devenyi, 2002: A generalized approach to parameterizing convection combining ensemble and data assimilation techniques. *Geophys. Res. Lett.*, **29(14),** Article 1693.

Hong, S.-Y., J. Dudhia, and S.-H. Chen, 2004: A Revised Approach to Ice Microphysical Processes for the Bulk Parameterization of Clouds and Precipitation, *Mon. Wea. Rev*., **132**, 103-120.

------, and H.-L. Pan, 1996: Nonlocal boundary layer vertical diffusion in a medium-range forecast model, *Mon. Wea. Rev*., **124**, 2322–2339.

Huffman, G.J., R.F. Adler, B. Rudolf, U. Schneider, and P.R. Keehn, 1995: Global precipitation estimates based on a technique for combining satellite-based estimates, rain gauge analysis, and NWP model precipitation information, *J. Climate*, **8**, 1284-1295.

------, 1997: Estimates of root-mean-square random error for finite samples of estimated precipitation, *J. Appl. Meteor.*, **36**, 1191-1201.

------, R.F. Adler, P. Arkin, A. Chang, R. Ferraro, A. Gruber, J. Janowiak, A. McNab, B. Rudolph, and U. Schneider, 1997: The global precipitation climatology project (GPCP) combined precipitation dataset, *Bull. Amer. Meteor. Soc.*, **78**, 5-20.

India Meteorological Office, 2007: Cyclones and depressions over the north Indian Ocean during 2006, *Mausam*, **58**, 3, 305-322.

Janjic, Z. I., 1994: The step-mountain eta coordinate model: further developments of the convection, viscous sublayer and turbulence closure schemes, *Mon. Wea. Rev.*, **122**, 927–945.

Janjic, Z. I., 2000: Comments on "Development and Evaluation of a Convection Scheme for Use in Climate Models", *J. Atmos. Sci.*, **57**, p. 3686.

Kain, J. S., and J. M. Fritsch, 1990: A one-dimensional entraining/ detraining plume model and its application in convective parameterization, *J. Atmos. Sci*., **47**, 2784–2802.

------, and ------, 1993: Convective parameterization for mesoscale models: The Kain-Fritcsh scheme, The representation of cumulus convection in numerical models, K. A. Emanuel and D.J. Raymond, Eds., *Amer. Meteor. Soc*., 246 pp.

Kalnay, E., and Coaurhtors, 1996: The NCEP/NCAR 40-Years Reanalysis Project. *Bull. Amer. Meteor. Soc.*, **77**, 437-471.

Lin, Y.-L., R. D. Farley, and H. D. Orville, 1983: Bulk parameterization of the snow field in a cloud model. J. Climate Appl. Meteor., 22, 1065–1092.

Krishnamurti, T. N., M. Kanamitsu, R. Godbole, C. B. Chang, F. Carr, and J. H. Chow, 1975: Study of a monsoon depression (I). Synoptic structure. *J. Meteor. Soc. Japan,* **53,** 227-239.

------, ------, ------, ------, ------, and ------, 1976: Study of a monsoon depression (II). Dynamical structure. *J. Meteor. Soc. Japan,* **54,** 208-225.

------, J. Molinari, H.-L. Pan, and V. Wong, 1977: Downstream amplification and formation of monsoon disturbances. *Mon. Wea. Rev.,* **105,** 1281-1297.

------, P.Ardanuy, Y. Ramanathan, and R.Pasch, and P.Greiman, 1980: Quick Look Summer MONEX Atlas Part III: Monsoon Depression Phase. FSU Report No. 80-8.

Mlawer, E. J., S. J. Taubman, P. D. Brown, M. J. Iacono, and S. A. Clough, 1997: Radiative transfer for inhomogeneous atmosphere: RRTM, a validated correlated-k model for the longwave. *J. Geophys. Res.*, **102 (D14)**, 16663–16682.

Moorthi, S., and A. Arakawa, 1985: Baroclinic instability with cumulus heating. *J. Atmos. Sci.,* **42,** 2007-2031.

Nitta, T., and K. Masuda, 1981: Observational study of a monsoon depression developed over the Bay of Bengal during Summer MONEX. *J. Meteor. Soc. Japan.*, **59**, 672–682.

Sabre, M., H. Hodges, K. Laval, J. Polcher, and F. Desalmand, 2000: Simulation of monsoon disturbances in the LMD GCM, *Mon. Wea. Rev*., **128**, 3752-3771.

Saha, K., and C.P. Chang, 1983: The Baroclinic Processes of Monsoon Depressions. *Mon. Wea. Rev.*, **111**, 1506–1514.

Skamarock, W. C., J. B. Klemp, J. Dudhia, D. O. Gill, D. M. Barker, W. Wang and J. G. Powers, 2005: A Description of the Advanced Research WRF Version 2, *NCAR Technical Note*, NCAR/TN-468+STR, 2005.

Shukla, J., 1978: CISK-barotropic-baroclinic instability and the growth of monsoon depressions. *J. Atmos. Sci.,* **35,** 495-508.

Sikka, D.R., 1977: Some aspects of the life history, structure and movement of monsoon depressions. *Pure Appl. Geophys.*, **115**, 1383-1412.

Warner, C., 1984: Core Structure of a Bay of Bengal Monsoon Depression. *Mon. Wea. Rev.*, **112**, 137–152.